© 2021. Published by The Company of Biologists Ltd | Development (2021) 148, dev197244. doi:10.1242/dev.197244

RESEARCH ARTICLE

A comprehensive series of Irx cluster mutants reveals diverse roles in facial cartilage development

D'Juan T. Farmer, Punam Patel, Rachelle Choi, Chih-Yu Liu and J. Gage Crump*

ABSTRACT

Proper function of the vertebrate skeleton requires the development of distinct articulating embryonic cartilages. Irx transcription factors are arranged in co-regulated clusters that are expressed in the developing skeletons of the face and appendages. *IrxB* cluster genes are required for the separation of toes in mice and formation of the hyoid joint in zebrafish, yet whether Irx genes have broader roles in skeletal development remains unclear. Here, we perform a comprehensive loss-of-function analysis of all 11 Irx genes in zebrafish. We uncover conserved requirements for *IrxB* genes in formation of the fish and mouse scapula. In the face, we find a requirement for *IrxAb* genes and *irx7* in formation of anterior neural crest precursors of the jaw, and for *IrxBa* genes in formation of endodermal pouches and gill cartilages. We also observe extensive joint loss and cartilage fusions in animals with combinatorial losses of Irx clusters, with *in vivo* imaging revealing that at least some of these fusions arise through inappropriate chondrogenesis. Our analysis reveals diverse roles for Irx genes in the formation and later segmentation of the facial skeleton.

KEY WORDS: Irx, Cartilage, Craniofacial skeleton, Fin, Zebrafish

INTRODUCTION

Development of the facial and limb skeletons follows a similar trajectory. Interactions of specialized epithelia with skeletogenic mesenchyme (neural crest-derived for the face, mesoderm-derived for the limb) promote proliferative outgrowth of mesenchyme followed by differentiation into a series of cartilage elements. These cartilages function primarily as transient templates for later bone differentiation, with permanent cartilage remaining at flexible joints between bones and in the nose, ear and trachea. Compared with cartilage specification, we know less about how individual cartilage elements are kept separate, both in the embryonic mesenchyme and later at joints.

Members of the Iroquois-related (Irx) transcription factor family are good candidates for maintaining cartilage separation during embryogenesis. Irx genes are required for the development of numerous organs, including the nervous system, heart, kidney and skeleton, and are thought to function generally as transcriptional repressors (Cavodeassi et al., 2001; Gomez-Skarmeta et al., 2001). The tetrapod *IrxA* cluster consists of *Irx1*, *Irx2* and *Irx4*, and the *IrxB* cluster consists of *Irx3*, *Irx5* and *Irx6*. In chickens and mice, *IrxA* and *IrxB* genes are expressed in the mesenchyme and perichondrium between nascent digit cartilages and in joint-forming regions (McDonald et al., 2010). The *Fused Toes* mouse mutant involves heterozygous deletion of the *IrxB* cluster (and three other genes) and is characterized by fusions of phalangeal foot bones (Grotewold and Ruther, 2002; Peters et al., 2002). In zebrafish, the *IrxB* gene *irx5a*, along with the fish-specific non-clustered *irx7*, are expressed at and required for development of the hyoid joint in the face, in part by blocking Sox9 activation of target genes such as *col2a1a* (Askary et al., 2015). *IrxB* genes also have earlier roles in formation of the limbs in mice, with proximal and anterior limb cartilages reduced in $Irx3^{-/-}; Irx5^{-/-}$ mice (Li et al., 2014). In addition, mice homozygous for the *Fused Toes* deletion, and hence lacking all *IrxB* genes, have hypoplastic pharyngeal arches, the embryonic structures populated by the neural crest-derived mesenchymal precursors of the facial skeleton (Anselme et al., 2007). In human Hamamy syndrome, dominant mutations in *IRX5* cause distinctive facial defects, with work in frog suggesting that Irx5 functions with Gata3 and Trps1 to regulate migration of the neural crest-derived precursors of the facial skeleton (Bonnard et al., 2012). In mice, *Irx3* and *Irx5* are also redundantly required for osteoblast differentiation in the cranium (Cain et al., 2016) and long bones (Tan et al., 2020).

Challenges in addressing Irx function include not only their iterative roles during development, e.g. early limb patterning (Li et al., 2014) versus later digit separation (Peters et al., 2002), but also genetic redundancy. Within and between clusters, Irx genes display similar and overlapping expression patterns, explained in part by super-enhancers that co-regulate Irx gene expression within a cluster (Tena et al., 2011). Zebrafish have 11 Irx genes, compared with six in tetrapods, which are organized into two *IrxA* clusters (*IrxAa*, *IrxAb*), two *IrxB* clusters (*IrxBa*, *IrxBb*), and the single fish-specific *irx7* gene, likely an evolutionary remnant of a third Irx cluster (Askary et al., 2015). We have taken advantage of the power of zebrafish genetics to mutate all Irx cluster genes and analyze the combinatorial requirements of individual Irx clusters. Phenotypic analysis reveals requirements of individual Irx clusters in body axis maintenance, heart development and skeletal development in the face and pectoral fin. We find a requirement for *IrxAb* and *irx7* genes in formation of the anterior facial skeleton in part by promoting the timely formation of cranial neural crest-derived cells (CNCCs). In contrast, *IrxBa* genes are required for formation of the posterior gill support skeleton in part by promoting the formation of endodermal pouches. Combinatorial Irx mutants also display widespread fusions of cartilages throughout the face, with *in vivo* imaging showing that inappropriate fusions between the lower jaw Meckel's and jaw support ceratohyal cartilages are due to inappropriate chondrogenesis of the perichondrium. Our work highlights evolutionarily conserved and redundant roles for Irx genes in the formation and individuation of cartilages throughout the body.

Eli and Edythe Broad California Institute for Regenerative Medicine Center for Regenerative Medicine and Stem Cell Research, Department of Stem Cell Biology and Regenerative Medicine, University of Southern California Keck School of Medicine, Los Angeles, CA 90033, USA.

*Author for correspondence (gcrump@usc.edu)

D.T.F., 0000-0002-3636-6835; J.G.C., 0000-0002-3209-0026

Handling Editor: Steve Wilson
Received 24 September 2020; Accepted 21 July 2021

Development (2021) 148, dev197244. doi:10.1242/dev.197244

RESULTS

Generation of a complete series of zebrafish Irx gene mutations

In order to understand requirements for the four clusters of Irx genes, we used Cas9 and multiple single guide RNAs (sgRNAs) (Hwang et al., 2013) to make small insertions or deletions that disrupt the open reading frame of each Irx gene, thus leading to truncated proteins lacking the conserved DNA-binding domains (Fig. 1A). We did not delete intervening regions between Irx genes in a cluster. Starting with the previously published *irx5a* mutant (Askary et al., 2015), we injected sgRNAs targeting both *irx3a* and *irx6a* and identified linked alleles with out-of-frame mutations in *irx3a*, *irx5a* and *irx6a* (‘*IrxBa*’ allele). Of the 23 injected animals that were screened, 18 had germline mutations in at least one gene, four had germline mutations in all *IrxBa* genes, and, of these, one had out-of-frame mutations in each and was used for phenotypic analysis. To generate the ‘*IrxBb*’ allele, we injected an sgRNA for *irx5b*, identified a founder for an *irx5b* mutant allele, and subsequently injected its progeny with *irx3b s*gRNA to generate linked *irx3b* and *irx5b* out-of-frame mutations. *IrxAa* and *IrxAb* alleles were created by simultaneously targeting all genes within each cluster (*irx1a*, *irx2a* and *irx4a* for *IrxAa*; *irx1b* and *irx4b* for *IrxAb*) and identifying founders with linked out-of-frame mutations for each cluster gene. For the *IrxAa* cluster, 48% of 19 injected and screened animals had single germline mutations, 33% two gene mutations and 19% three gene mutations, with one out of ten of the

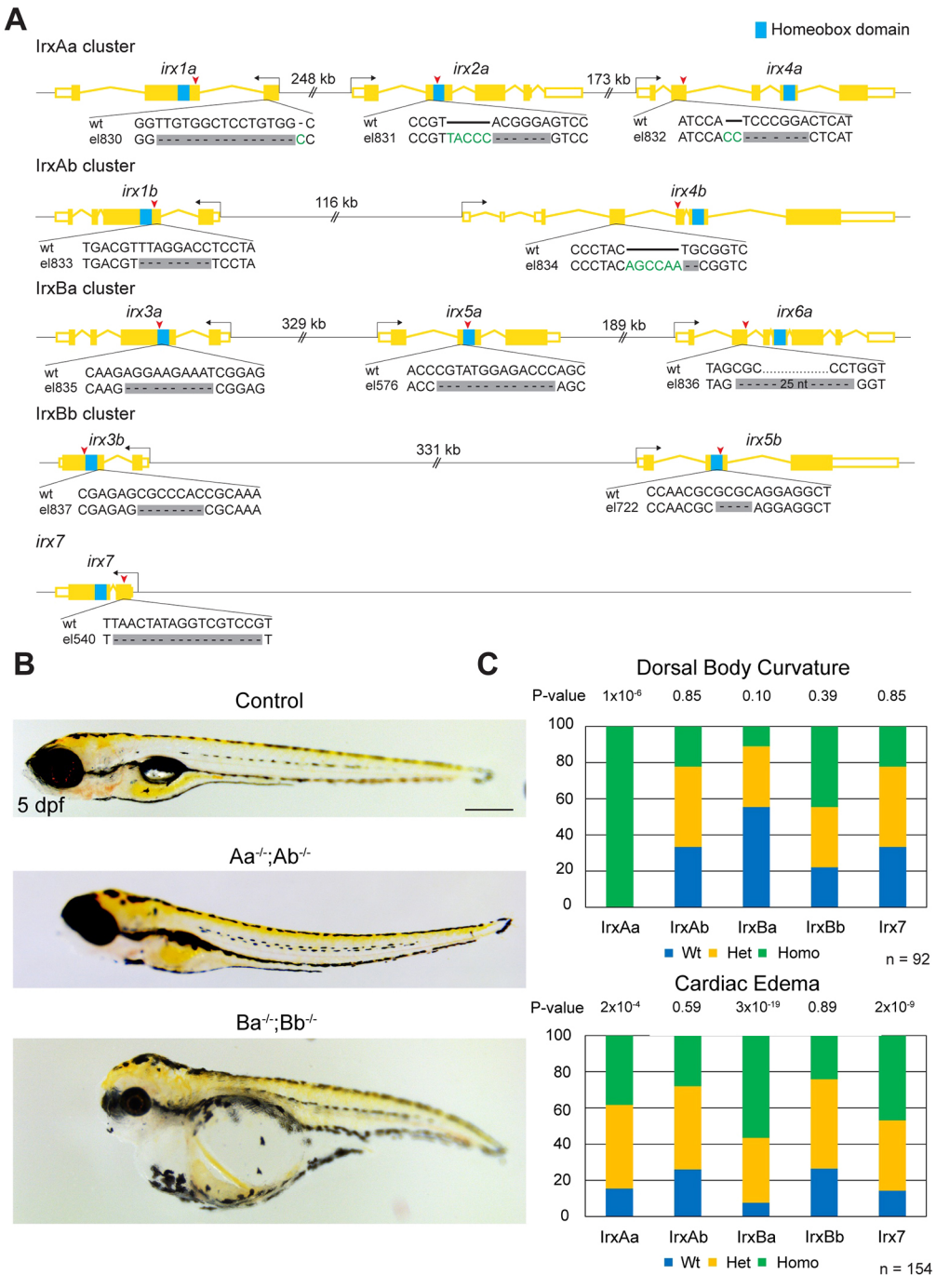

Fig. 1. Generation of a complete series of Irx cluster mutants in zebrafish. (A) Schematic of CRISPR/Cas9 strategy to generate Irx cluster mutants. All selected alleles result in frame-shift mutations (red arrowheads). Dashes indicate deleted nucleotides, and green letters indicate insertions. All alleles are predicted to delete or truncate the DNA-binding homeobox domain (blue box). (B) Brightfield images showing dorsal axis curvature in the absence of *IrxA* genes and cardiac edema in the absence of *IrxB* genes. (C) Summary of genotypes for the indicated phenotypes from a quintuple heterozygous in-cross. *P*-values report chi-square tests for deviation from the expected 1:2:1 wild type:heterozygous: homozygous Mendelian ratio. Scale bar: 1 mm.

Development (2021) 148, dev197244. doi:10.1242/dev.197244

triple mutant founders having out-of-frame indels in each *IrxAa* gene and used for further analysis. For the *IrxAb* cluster, 54% of injected and screened animals had single germline mutations and 46% had mutations in both genes; three out of four double mutants had out-of-frame indels in both genes, with one allele used for further analysis. Our findings reveal that multiple genes within a cluster can be simultaneously targeted at reasonably high efficiency, without large deletions, in a single generation.

Body axis defects, cardiac edema and lethality in Irx cluster mutants

Animals with homozygous mutations in *IrxAa* or *IrxBa* clusters failed to inflate swim bladders and did not survive beyond 7 days post-fertilization (dpf). For *IrxBa*$^{-/-}$ mutants, this reflects a role of *irx3a* and/or *irx6a* in survival as single *irx5a* mutants survive to adulthood (Askary et al., 2015). Homozygous *IrxAb* or *IrxBb* cluster mutants developed normally and were adult viable. To resolve comprehensively the diverse requirements of Irx genes during embryonic development, we performed in-crosses of quintuple heterozygous zebrafish (*IrxAa*$^{+/-}$; *IrxAb*$^{+/-}$; *IrxBa*$^{+/-}$; *IrxBb*$^{+/-}$; *irx7*$^{+/-}$). In total, we collected 2081 embryos from 13 clutches. Animals that failed to inflate their swim bladders by 4 dpf were collected, visually inspected for abnormalities, and processed for staining of cartilage (Alcian Blue) and bone (Alizarin Red). To determine the genetic drivers for gross and skeletal phenotypes, ∼500 embryos were categorized by phenotype and genotyped. A subset of embryos developed dorsal curvature of the body axis between 3 and 5 dpf, which correlated with abnormal circling behavior at 5 dpf. These phenotypes were driven primarily by *IrxAa* loss, although *IrxAa*$^{+/-}$; *IrxAb*$^{-/-}$ mutants often displayed a similar abnormal circling behavior as adults (Fig. 1B,C, Fig. S1A, Movie 1). Circling behavior seems unlikely to be due to vestibular defects as semicircular canals were unaffected in *IrxAa*$^{-/-}$; *IrxAb*$^{-/-}$ mutants at 6 dpf (Fig. S1B). *IrxAa*$^{-/-}$; *IrxAb*$^{-/-}$ mutants also displayed an abnormal jaw gape (Fig. S1C, Movie 2). As we failed to detect any abnormalities in jaw cartilages, joint structures, muscles and *isl1*:*GFP*$^{+}$ motor nerves innervating these muscles at 6 dpf (Fig. S1D-F), abnormal jaw gape might instead reflect the known role of Irx genes in patterning the central nervous system (Cavodeassi et al., 2001). Progeny of quintuple heterozygous in-crosses also developed cardiac edema (Fig. 1B), which was attributable to mutations in *IrxAa*, *IrxBa* and *irx7* (Fig. 1B,C), consistent with published roles for *IrxA* and *IrxB* cluster genes in heart development (Kim et al., 2012).

Proximal cartilage defects in the pectoral fins of *IrxB* cluster mutants

Irx genes play crucial roles in limb development (Grotewold and Ruther, 2002), and the fish pectoral fin is homologous to the mammalian forelimb. We observed Irx mutants with severe reductions of the scapulocoracoid cartilage, a major component of the proximal pectoral fin (Fig. 2A). The postcoracoid process, the posterior element in the proximal fin, and the endochondral disc of the distal fin were relatively unaffected. This phenotype resembles loss of the scapula, the proximal-most portion of the forelimb, in mice lacking *IrxB* genes (*Irx3*, *Irx5*) (Li et al., 2014). Pectoral fin defects were solely attributable to *IrxBa* loss (Fig. 2B). This conservation of *IrxB* gene function further supports proximal-distal identity being an ancestral feature of the fish pectoral fin that predates evolution of the tetrapod limb (Gehrke et al., 2015) (Fig. 2C).

Distinct Irx requirements for formation of the anterior versus posterior facial skeleton

In addition to fin defects, we identified mutant zebrafish with reduced or absent facial cartilages. Three major classes emerged

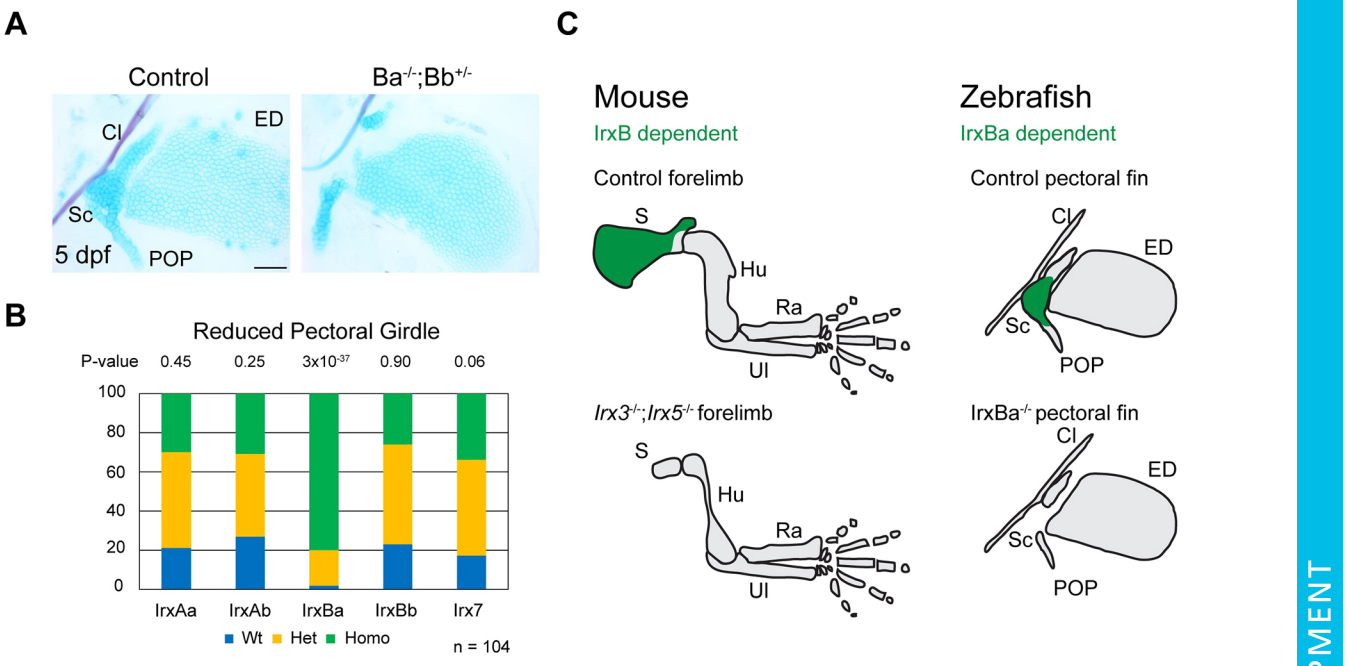

Fig. 2. Requirement for *IrxB* genes in pectoral fin development. (A) Alcian Blue (cartilage) and Alizarin Red (bone) staining of pectoral fins shows reductions of the scapulocoracoid cartilage in *IrxBa*$^{-/-}$; *IrxBb*$^{+/-}$ mutants. (B) Summary of genotypes for the reduced pectoral girdle phenotype from a quintuple heterozygous in-cross. *P*-values report chi-square tests for deviation from the expected 1:2:1 wild type:heterozygous:homozygous Mendelian ratio. (C) Model highlighting the conserved roles of *IrxB* genes in development of proximal structures of the mouse forelimb and zebrafish pectoral fin. Green shading indicates regions for which development is dependent on *IrxB*/*IrxBa*. Cl, cleithrum; ED, endoskeletal disc cartilage; Hu, humerus; POP, postcoracoid process; Ra, radius; S, scapula; Sc, scapulocoracoid cartilage; Ul, ulna. Scale bar: 100 µm.

Development (2021) 148, dev197244. doi:10.1242/dev.197244

(Fig. 3). The first lacked the anterior facial skeleton, including the Meckel's and palatoquadrate cartilages, which was driven by *IrxAb* and *irx7* loss. The second lacked the posterior ceratobranchial cartilages, attributable to *IrxBa* and *irx7* loss, with enhanced severity induced by *IrxBb* loss (Fig. 3A,B, Fig. S2A). The final group was characterized by a near-complete loss of facial cartilages, including a reduced/absent neurocranium (Fig. 3A,B, Fig. S2B,C), which was driven by mutations in *IrxAb*, *IrxBa*, *irx7* and, to a modest degree, *IrxBb*; 14/15 zebrafish with 9/10 Irx cluster alleles deleted had widespread loss of facial cartilages. We failed to recover any embryos at 4 dpf completely lacking all 11 Irx genes ($IrxAa^{-/-}$; $IrxAb^{-/-}$; $IrxBa^{-/-}$; $IrxBb^{-/-}$; $irx7^{-/-}$). This could reflect the previously reported expression of *irx7* during early gastrulation (Satija et al., 2015), and hence early lethality, or alternatively failure to screen enough progeny from all-heterozygous in-crosses (0/2081 analyzed versus expected frequency of 1/1024, P=0.07, one-tailed Student's t-test).

The jaw cartilages derive from the most anterior pharyngeal arch, the mandibular, and the ceratobranchial cartilages from the five most posterior arches, the branchials. To understand better the facial cartilage losses in Irx mutants, we assessed earlier pharyngeal arch development (Fig. 3C). In $IrxAb^{-/-}$; $irx7^{-/-}$ mutants, we observed a near-complete loss of *sox10:dsRed*$^{+}$ CNCCs of the mandibular arch, a reduction in CNCCs of the hyoid (second) arch, but little change in branchial CNCCs at 36 hours post-fertilization (hpf). Re-imaging of the same individuals at 4 dpf confirmed that these

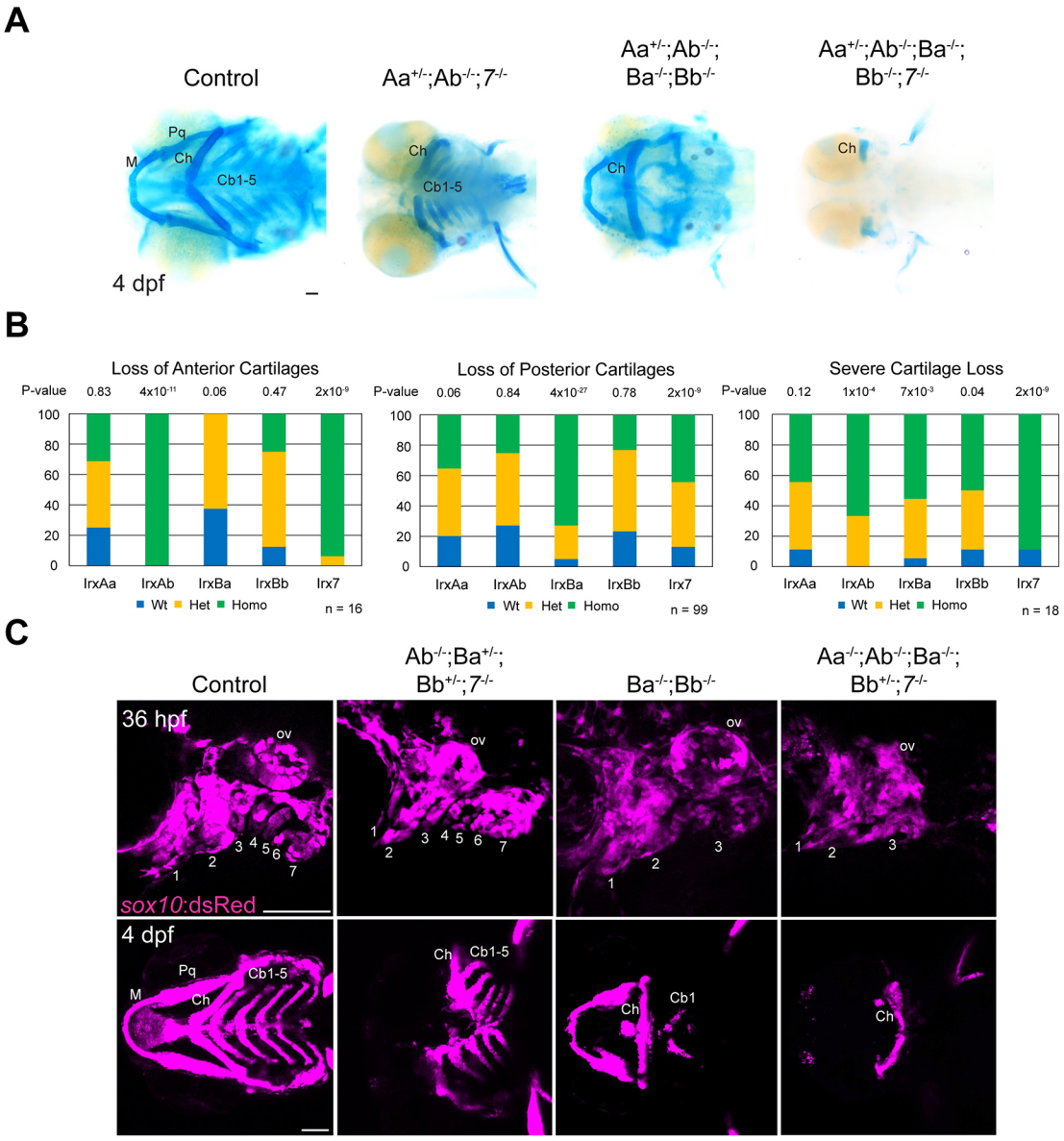

Fig. 3. Facial cartilage reductions in Irx mutants. (A) Ventral views of larvae stained with Alcian Blue (cartilage). Three phenotypic groups were identified in Irx mutants: anterior cartilage loss (left), posterior cartilage loss (middle), and near-complete cartilage loss (right). (B) Summary of genotypes for the indicated phenotypes from a quintuple heterozygous in-cross. *P*-values report chi-square tests for deviation from the expected 1:2:1 wild type:heterozygous:homozygous Mendelian ratio. (C) Sequential confocal imaging of individual zebrafish shows that reductions of the first and second arches (numbered) precede loss of mandibular cartilages (left), reductions of posterior arches 3-7 precede absence of ceratobranchial cartilages (middle), and reductions of all arches precede severe cartilage loss (right). Genotypes of specific examples are shown. Cb1-5, ceratobranchials 1-5; Ch, ceratohyal; M, Meckel's; ov, otic vesicle; Pq, palatoquadrate. Scale bars: 100 µm.

Development (2021) 148, dev197244. doi:10.1242/dev.197244

early arch patterning defects precede the specific loss of jaw cartilages. Reciprocally, *IrxBa*$^{-/-}$; *IrxBb*$^{-/-}$ mutants displayed reduced branchial arches 3-7 yet relatively normal mandibular and hyoid arch CNCCs at 36 hpf, which correlated with severe loss of ceratobranchial cartilages when re-imaged at 4 dpf. Irx mutants with 9/10 alleles deleted displayed a near-complete loss of *sox10:dsRed*$^{+}$ CNCCs in the mandibular arch, a poorly formed hyoid arch, and reduced arches 3-7, which correlated with large-scale loss of facial cartilages, with the exception of the ceratohyal, at 4 dpf. These findings reveal region-specific roles for *IrxA* and *IrxB* genes in the formation of the anterior and posterior pharyngeal arches, respectively.

Reduced specification of anterior CNCCs in *IrxAb*$^{-/-}$; *irx7*$^{-/-}$ mutants

In order to determine the origins of pharyngeal arch defects in Irx mutants, we examined a time course of CNCC development. In wild-type embryos at 11 hpf, expression of *sox10* labels premigratory neural crest cells at the neural plate border. In *IrxAb*$^{-/-}$; *irx7*$^{-/-}$ mutants, we observed a near-complete loss of *sox10* expression in the presumptive neural crest domain at this stage (Fig. 4A). In wild-type embryos at 16.5 hpf, expression of *dlx2a* labels the neural crest-derived ectomesenchyme precursors of the craniofacial skeleton that have begun to migrate toward the pharyngeal arches in three streams. In *IrxAb*$^{-/-}$; *irx7*$^{-/-}$ mutants, *dlx2a* expression, particularly in the first (mandibular) stream, was reduced (Fig. 4B). A similar and preferential loss of mandibular CNCCs in *IrxAb*$^{-/-}$; *irx7*$^{-/-}$ mutants was seen with the pan-neural crest transgene *sox10*:*dsRed* at 16.5 hpf, showing a requirement for *IrxAb* and *irx7* for the generation of CNCCs and not the ectomesenchyme identity of mandibular arch CNCCs (Fig. 4C, Fig. S3). In contrast, no notable differences in *dlx2a* expression or the number of *sox10*:*dsRed*$^{+}$ cells were apparent in *IrxBa*$^{-/-}$ mutants (which display reduced gill cartilages) at 16.5 hpf. By 24 hpf, quantification of *sox10*:*dsRed*$^{+}$ cells revealed a 50% reduction in the number of mandibular arch CNCCs in *IrxAb*$^{-/-}$; *irx7*$^{-/-}$ mutants, with no statistical

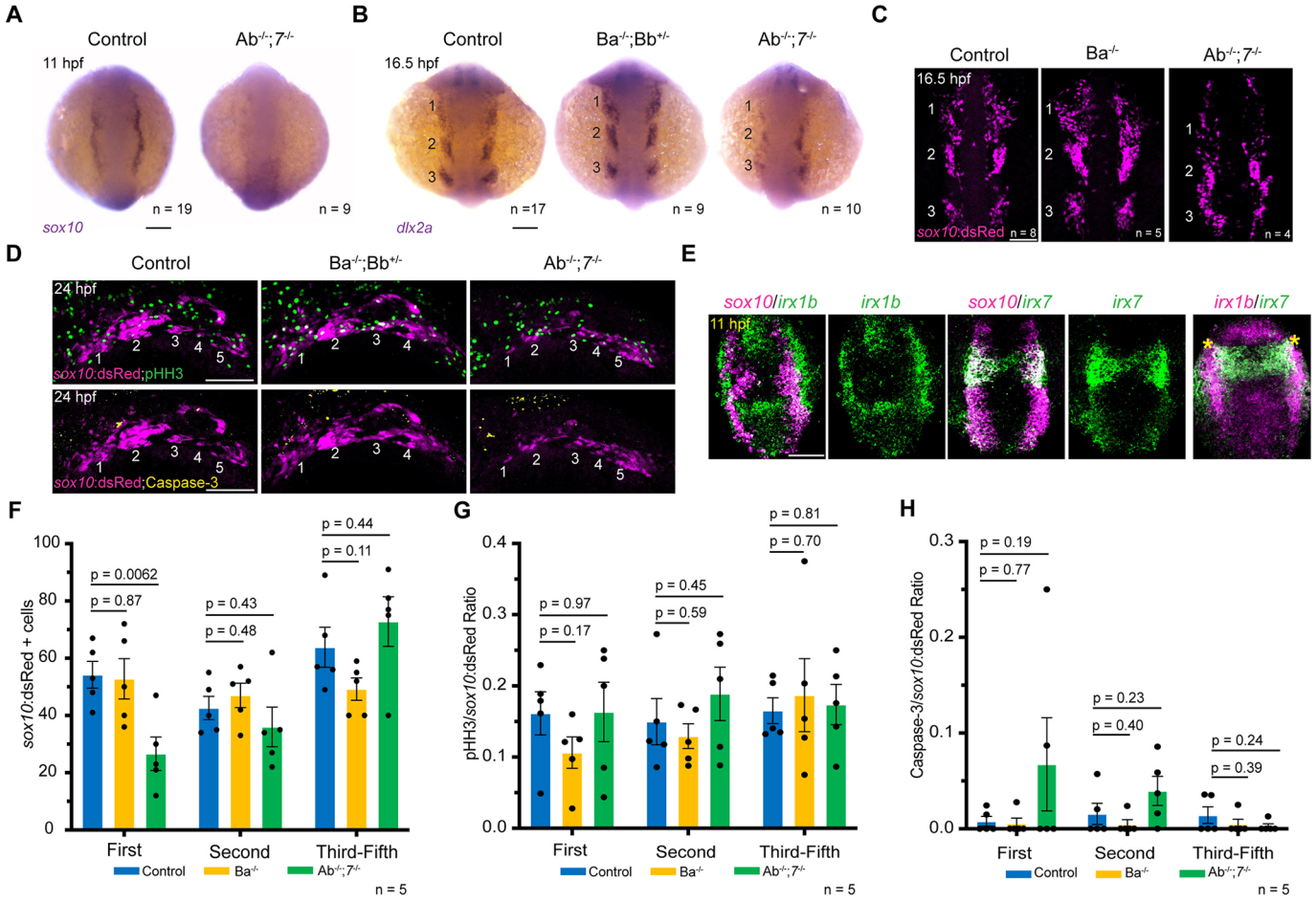

Fig. 4. Impaired CNCC development in *IrxAb*; *irx7* mutants. (A) Expression of the CNCC marker *sox10* is severely reduced in *IrxAb*$^{-/-}$; *irx7*$^{-/-}$ mutants at 11 hpf. (B) At 16.5 hpf, *dlx2a* expression marks three streams of neural crest ectomesenchyme (numbered) in wild-type controls. Expression of *dlx2a* is reduced in *IrxAb*$^{-/-}$; *irx7*$^{-/-}$ mutants, especially in the first stream, but unaffected in *IrxBa*$^{-/-}$; *IrxBb*$^{+/-}$ mutants. (C) *sox10*:*dsRed* marks three streams of CNCCs at 16.5 hpf. The first stream is preferentially reduced in *IrxAb*$^{-/-}$; *irx7*$^{-/-}$ mutants but unaffected in *IrxBa*$^{-/-}$ mutants. (D) *sox10*:*dsRed* labels five pharyngeal arches in wild-type controls and *IrxBa*$^{-/-}$; *IrxBb*$^{+/-}$ mutants, but only four arches in *IrxAb*$^{-/-}$; *irx7*$^{-/-}$ mutants. Immunostaining shows proliferating cells (phospho-histoneH3^{+}, pHH3) and apoptotic cells (Caspase-3^{+}). (E) *In situ* hybridizations at 11 hpf show co-expression of *irx1b* and *irx7* in CNCCs (asterisks), with partial overlap with the neural crest marker *sox10*. There is also strong expression of *irx1b* in the pre-placodal domain just lateral to the *sox10*$^{+}$ neural crest domain. (F-H) Quantification of *sox10*:*dsRed*$^{+}$ cells, proportion of pHH3^{+} to *sox10*:*dsRed*$^{+}$ cells, and Caspase-3^{+} to *sox10*:*dsRed*$^{+}$ cells within the first, second and posterior pharyngeal arches of the indicated genotypes at 24 hpf. *P*-values were calculated using two-tailed non-parametric Student's *t*-tests. Error bars represent s.e.m. *n* denotes individual embryos in which the indicated patterns were observed. Scale bars: 100 µm.

Development (2021) 148, dev197244. doi:10.1242/dev.197244

differences in hyoid and branchial neural crest-derived cells (Fig. 4D,F). We also failed to detect any changes in phospho-histoneH3^{+} proliferative or Caspase-3^{+} apoptotic arch CNCCs in *IrxAb*$^{-/-}$; *irx7*$^{-/-}$ or *IrxBa*$^{-/-}$ mutants at 24 hpf (Fig. 4D,G,H). Consistent with an early role for *IrxAb* genes and *irx7* for the formation of CNCCs, we observed *irx1b* and *irx7* expression within *sox10*$^{+}$ premigratory neural crest cells at 11 hpf, as well as stronger *irx1b* expression in the pre-placodal region (Fig. 4E). Our analysis points to roles for *IrxAb* and *irx7* genes, but not *IrxBa* genes, in the timely specification of CNCCs, with defects in this process resulting in the later preferential loss of mandibular arch CNCCs and the anterior facial skeleton.

Requirements for *IrxBa* genes in pharyngeal pouch formation

As we found that the loss of gill cartilages in *IrxBa*$^{-/-}$ mutants was not the consequence of defects in the early specification, migration, proliferation or survival of posterior arch CNCCs, we next examined development of the pharyngeal pouches. Although formation of endodermal pouches is largely independent of CNCCs (Cox et al., 2012; Veitch et al., 1999), loss of pouches is known to secondarily disrupt the survival of posterior arch CNCCs and the formation of gill cartilages (David et al., 2002; Piotrowski et al., 2003). At 16.5 hpf, a stage prior to the onset of pouch morphogenesis, we observed no changes in *her5*:*GFP*$^{+}$ endoderm and *sox10*:*dsRed*$^{+}$ CNCCs of *IrxBa*$^{-/-}$; *IrxBb*$^{+/-}$ mutants versus wild-type siblings (Fig. 5A). By 24 hpf, however, when wild types have developed three pouches, we observed only a rudimentary first and second pouch in *IrxBa*$^{-/-}$; *IrxBb*$^{+/-}$ mutants, and this correlated with a failure to properly segment the posterior-most neural crest-derived stream (Fig. 5B). These phenotypes became more apparent by 36 hpf, with six pouches in wild types and only rudimentary first and second pouches in mutants, which correlated with a reduction in and failure to segment the posterior arch CNCCs (Fig. 5C). In addition, the lack of gill cartilage defects in *irx5a* single mutants (Askary et al., 2015) indicates roles for *irx3a* and/or *irx6a* in pouch formation. Consistent with such roles, we observed expression of *irx3a* in the posterior arches at 24 hpf, both within *dlx2a*$^{+}$ CNCCs and *dlx2a*$^{-}$ cells that could be endoderm and/or mesoderm (Fig. 5D). Although further studies are needed to determine in which tissues *IrxBa* genes are required, our data reveal roles for *IrxBa* genes in pouch formation that likely contribute to the selective loss of gill cartilages.

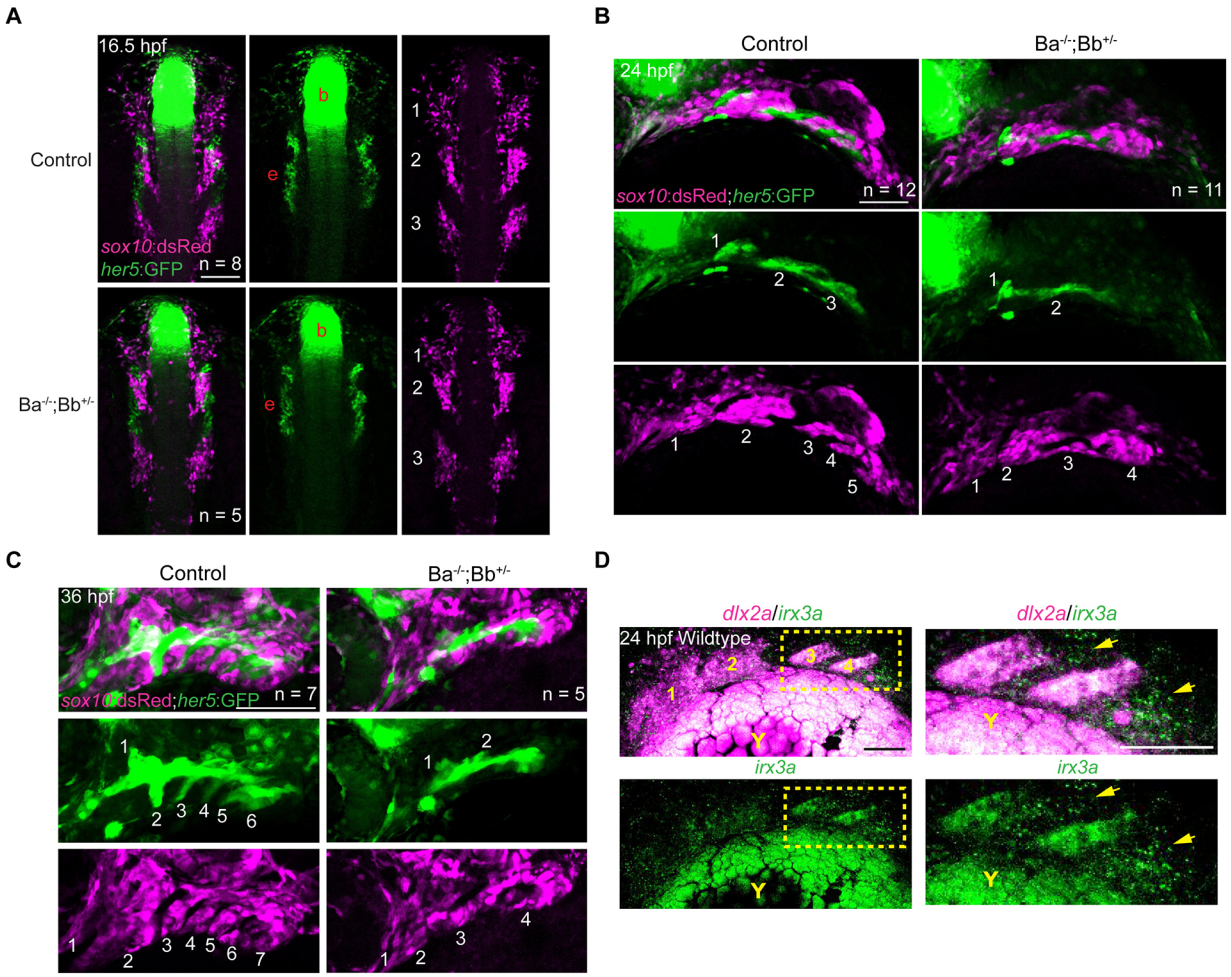

Fig. 5. Requirement of *IrxB* genes for pharyngeal pouch formation. (A) Confocal images show three bilateral streams of *sox10*:*dsRed*$^{+}$ CNCCs (numbered) and *her5*:*GFP*$^{+}$ endoderm in wild-type sibling controls and *IrxBa*$^{-/-}$; *IrxBb*$^{+/-}$ mutants at 16.5 hpf. (B,C) Lateral views show loss of *her5*:*GFP*$^{+}$ posterior pouches (green, numbered) and reduced numbers of *sox10*:*dsRed*$^{+}$ neural crest-derived arches (magenta, numbered) in *IrxBa*$^{-/-}$; *IrxBb*$^{+/-}$ mutants versus wild-type sibling controls at 24 and 36 hpf. (D) *In situ* hybridization reveals co-expression of *irx3a* with the ectomesenchyme marker *dlx2a* in the third and fourth pharyngeal arch, as well as the intervening *dlx2a*-negative regions (arrows) where endodermal pouches are located. Boxed region is magnified on the right. b, brain; e, endoderm; Y, yolk. *n* numbers denote individual embryos in which the indicated patterns were observed. Scale bars: 100 µm.

Development (2021) 148, dev197244. doi:10.1242/dev.197244

Widespread facial cartilage fusions and joint loss in compound Irx mutants

In addition to cartilage loss, we also uncovered Irx mutant combinations displaying widespread fusions of facial cartilages, both across joints and between neighboring cartilages (Fig. 6A-D). Consistent with our previous data that loss of the *IrxBa* cluster gene *irx5a* enhanced hyoid joint defects in *irx7* mutants (Askary et al., 2015), loss of *irx7*, and to a lesser extent the *IrxBa* cluster, resulted in fusions across the hyoid joint and truncation of the adjacent symplectic cartilage (Fig. 6E,K). We also observed fusions across the jaw joint (Fig. 6F,L; attributable to *IrxAb* and *irx7* mutations) and across the midline joint between the two lower jaw Meckel's

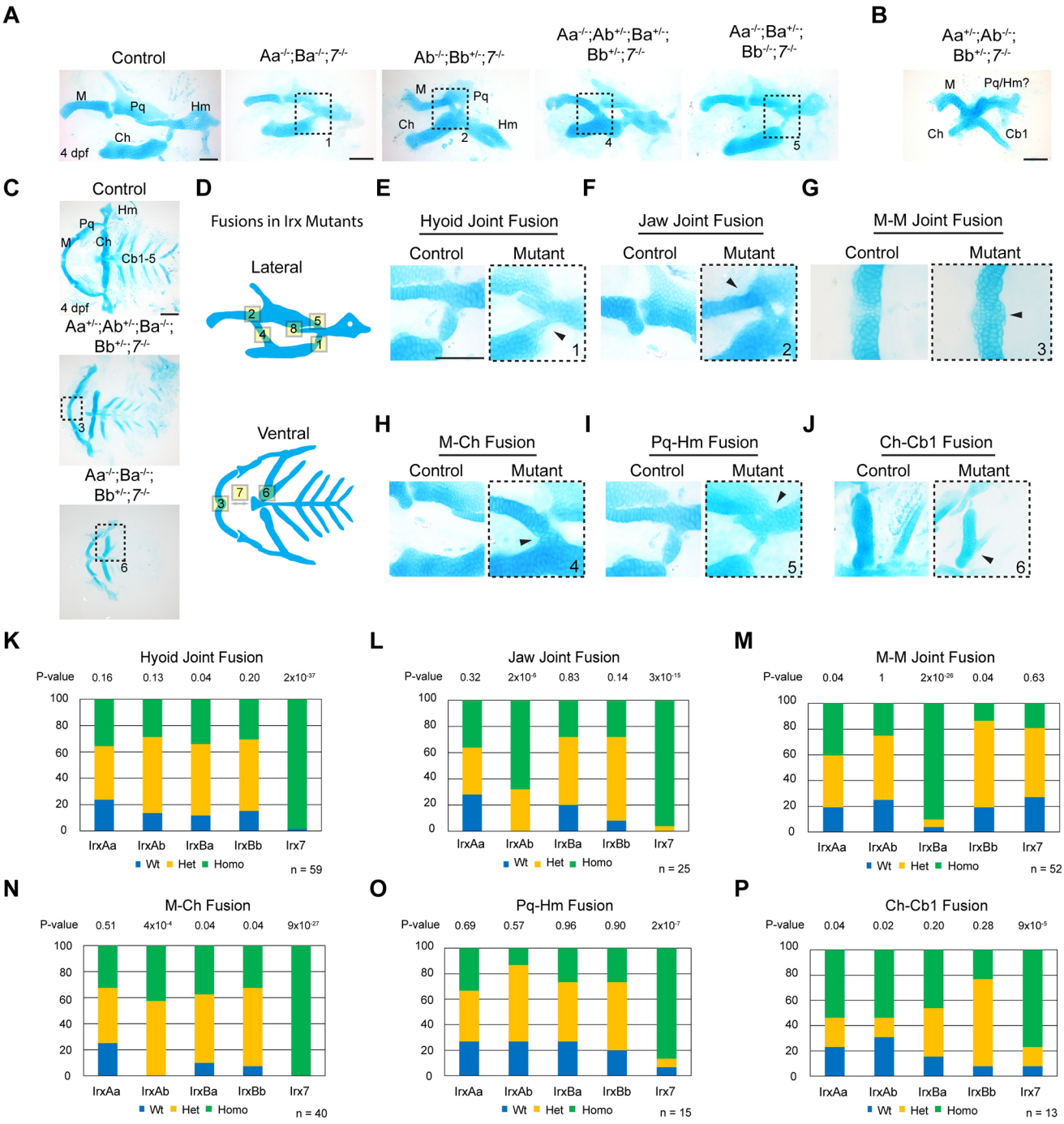

Fig. 6. Widespread facial cartilage fusions and joint loss in Irx mutants. (A,B) Dissected first and second arch-derived skeletons shown in lateral view and stained with Alcian Blue (cartilage) at 4 dpf. Distinct combinations of Irx mutations result in a range of cartilage fusions and joint loss (boxed regions) (A), and in severe cases fusions of multiple cartilages (B). (C) Dissected facial cartilages shown in ventral view, with dashed boxes showing cartilage fusions. (D) Schemes of the range of cartilage fusions and joint losses seen in Irx mutant combinations. Numbers correspond to the boxed regions in A and C; see Fig. S4 for fusions 7 and 8. (E-J) Magnifications of the cartilage fusions seen in A and C (boxed regions) versus similar regions from wild-type controls. (K-P) Summary of genotypes for the indicated phenotypes from a quintuple heterozygous in-cross. *P*-values report chi-square tests for deviation from the expected 1:2:1 wild type:heterozygous: homozygous Mendelian ratio. *n* denotes animals in which the indicated fusions were observed. Cb, ceratobranchial; Ch, ceratohyal; Hm, hyomandibular; M, Meckel's; Pq, palatoquadrate. Scale bars: 100 µm.

Development (2021) 148, dev197244. doi:10.1242/dev.197244

cartilages (i.e. mandibular symphysis; Fig. 6G,M; attributable to *IrxBa* mutations). In more severe cases of Meckel's-Meckel's midline fusions, the tips of the lower jaw cartilages project posteriorly (Fig. S4A,B; attributable to *IrxBa* and *irx7* loss). In addition to joint fusions, we also observed fusions of cartilages derived from neighboring arches, including Meckel's and ceratohyal (Fig. 6H,N; attributable to *IrxAb* and *irx7* loss, and to a lesser extent *IrxBa* and *IrxBb* mutations), palatoquadrate and hyomandibula (Fig. 6I,O; attributable to *irx7* mutations), ceratohyal and ceratobranchial 1 (Fig. 6J,P; attributable to *irx7*, and to a lesser extent *IrxAa* and *IrxAb* mutations), Meckel's and basibranchial (Fig. S4C-E; attributable to *IrxBa*, *IrxBb* and *irx7* mutations), and, rarely, palatoquadrate and symplectic (Fig. S4F; genotypes not defined). In the most severe cases, we observed fusions of cartilages of the first three arches (Meckel's, palatoquadrate, ceratohyal, hyosympletic and the first ceratobranchial) into a single mass (Fig. 6B).

In order to understand the etiology of cartilage fusions, we examined earlier pharyngeal arch development in *IrxBa*$^{+/-}$; *IrxBb*$^{-/-}$; *irx7*$^{-/-}$ mutants; these animals lack the confounding cardiac edema associated with non-specific reductions of the head skeleton observed in *IrxBa* homozygous mutants. Of three *IrxBa*$^{+/-}$; *IrxBb*$^{-/-}$; *irx7*$^{-/-}$ mutants displaying normal pouches separating *sox10:dsRed*$^{+}$ arch CNCCs at 36 hpf, re-imaging at 4 dpf confirmed that all individuals developed Meckel's-ceratohyal fusions (Fig. S4G). Serial live imaging of *IrxBa*$^{+/-}$; *IrxBb*$^{-/-}$; *irx7*$^{-/-}$ mutants with Meckel's-ceratohyal fusions revealed that 8/8 displayed earlier ectopic outgrowths of *sox10:dsRed*$^{+}$ cells from the ceratohyal cartilage at 60 hpf, with these outgrowths fusing with Meckel's cartilage between 72 and 96 hpf in all cases examined (Fig. 7A). Examination of an *irx7:GFP* knock-in reporter line revealed expression in the ceratohyal perichondrium where outgrowths and eventual fusions to Meckel's cartilage occur (Fig. S5). We also performed imaging of *IrxBa*; *IrxBb*; *irx7* mutants double-positive for *trps1*:*GFP*, which is expressed at higher levels in the perichondrium versus cartilage at 5 dpf, and the cartilage marker *sox10*:*dsRed*. Among the seven mutants identified with ectopic cartilage along the ceratohyal, five displayed a severe Meckel's-ceratohyal fusion, one a mild fusion, and one an unfused outgrowth from the ceratohyal in the same region in which fusions to Meckel's typically occur in mutants (Fig. 7B). On the side of the ceratohyal that typically fuses to Meckel's, we observed a mixture of *trps1*:*GFP*^{high}; *sox10*:*dsRed*$^{+}$ and *trps1*:*GFP*^{low}; *sox10*:*dsRed*$^{+}$ cells in the mutant perichondrium, with many having a flattened appearance typical of wild-type *trps1*:*GFP*^{high}; *sox10*:*dsRed*$^{-}$ perichondral cells. In the mild fusion example, cells at the fusion site were *trps1*:*GFP*^{high}; *sox10*:*dsRed*$^{+}$. Our findings suggest that, in addition to preventing inappropriate cartilage maturation in the hyoid joint (Askary et al., 2015), Irx7 and IrxB family members also function to prevent inappropriate chondrogenesis in the perichondrium, although we cannot rule out the possibility that proliferative expansion of chondrocytes alternatively or also contributes to mutant fusions (Fig. 7C).

DISCUSSION

Here, we uncover diverse roles for Irx proteins in the development of the facial and fin skeletons of zebrafish. The common loss of the most proximal skeletal element in the *IrxBa* mutant pectoral fin (scapulocoracoid) and the *Irx3/Irx5* mutant forelimb (scapula) indicate common requirements for *IrxB* genes in these homologous appendages. Interestingly, *IrxA* and *IrxB* clusters appear to play largely distinct roles in facial development. We find that loss of jaw cartilages in *IrxAb*$^{-/-}$; *irx7*$^{-/-}$ mutants is due to preferential defects in the specification of the anterior-most skeletogenic CNCCs. In contrast, *IrxB* genes play a role in formation of the endodermal pouches required for gill cartilage formation.

The role of *IrxA* genes in zebrafish neural crest formation appear to be distinct from what has been reported in mouse and frog. In *Fused toes* mice with homozygous deletion of the *IrxB* cluster, the pharyngeal arches are hypoplastic at embryonic day 10.5, and this correlates with a reduction in expression of the neural crest marker *Sox10* at earlier stages (Anselme et al., 2007). In *Xenopus laevis*, morpholino knockdown of the *IrxB* gene *Irx5* was suggested to affect the migration rather than specification of CNCCs, although, as in zebrafish *IrxAb*$^{-/-}$; *irx7*$^{-/-}$ mutants, neural crest defects were more pronounced in the anterior head (Bonnard et al., 2012). It will be interesting to investigate whether Irx proteins promote mesenchyme development through a similar mechanism in the face as reported for Irx3 and Irx5 in appendages, for example by interacting with Shh signaling (Li et al., 2014) and controlling chromatid segregation (Tao et al., 2020).

Our findings suggest that it is the expression domains rather than the protein functions of individual Irx clusters that account for their regional requirements in the skeleton, and that reductions in Irx genes impact facial skeleton formation by affecting the earlier development of both the skeletogenic ectomesenchyme and the pharyngeal pouches. Although we lacked the resources to analyze contributions of individual members of each Irx cluster, we note that the larval lethality and pouch defects observed in *IrxBa*$^{-/-}$ mutants were not seen when only *irx5a* was mutated (Askary et al., 2015), indicating roles for the two other members of the *IrxBa* cluster (*irx3a* and *irx6a*) in these processes. Hence, the general co-regulation of genes within an Irx cluster, combined with our combinatorial analysis of all Irx cluster deletions, would support genetic redundancy both within and across Irx clusters for patterning the vertebrate skeleton.

By analyzing all possible combinations of Irx cluster loss, we were also able to uncover mutant animals that developed later fusions of cartilages as opposed to earlier losses of CNCCs and pouches. These fusions included those between neighboring facial cartilages, reminiscent of the fusions of the toe bones seen in the *Fused toes* mouse mutant. Whereas toe fusion had been proposed to occur through a loss of programmed cell death between digits (van der Hoeven et al., 1994), *in vivo* imaging in zebrafish revealed that fusion between the lower jaw Meckel's and the ceratohyal cartilages, which form from distinct pharyngeal arches, occurs through ectopic chondrogenesis. A requirement for *irx7* mutations for this type of fusion is consistent with expression of *irx7:GFP* in the region of the ceratohyal perichondrium undergoing inappropriate chondrogenesis in mutants, and more generally with the expression of multiple Irx genes in the perichondrium and joint-forming regions of the avian and murine autopod (McDonald et al., 2010). Previous data had shown that Irx5a and Irx7 ensure formation of the hyoid joint by suppressing the ability of Sox9 to activate target genes and promote cartilage maturation (Askary et al., 2015). It will therefore be interesting to explore whether Irx proteins act in a similar manner to prevent cartilage formation in the perichondrium. In addition to loss of the hyoid joint and fusion of Meckel's and ceratohyal cartilages, we observed numerous other joint losses and cartilage fusions in Irx mutant combinations. It remains unclear which particular Irx members are expressed in these other zones of cartilage fusions. Moreover, it is possible that some of these other fusions are indirect consequences of earlier defects, such as reduced CNCCs. Indeed, reductions of mandibular

Development (2021) 148, dev197244. doi:10.1242/dev.197244

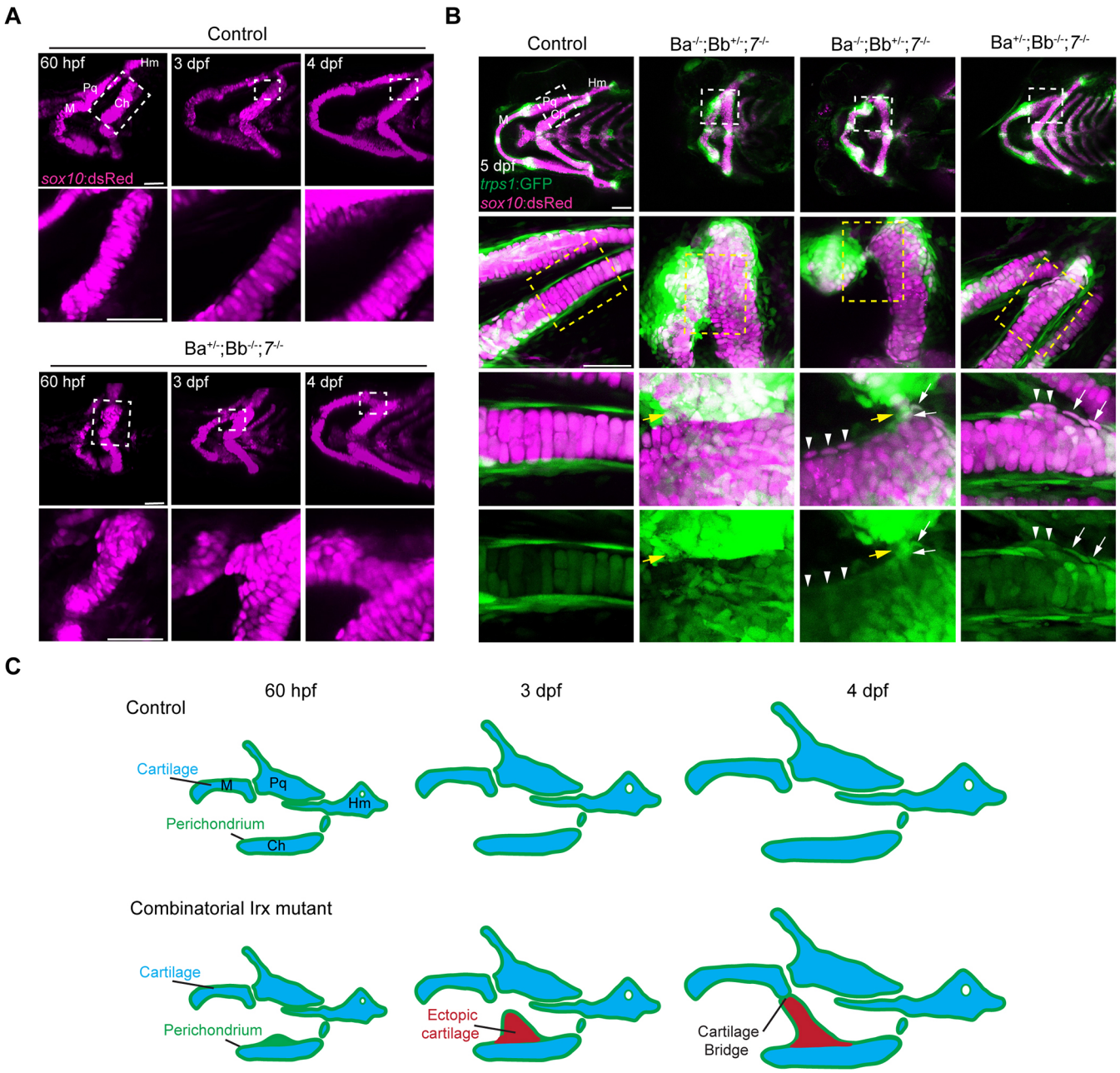

Fig. 7. Sequential *in vivo* imaging of cartilage fusion in Irx mutants. (A) Serial confocal imaging of *sox10*:*dsRed*$^{+}$ facial cartilages in wild-type sibling controls and *Irx*Ba$^{+/-}$; *Irx*Bb$^{-/-}$; *irx7*$^{-/-}$ mutant embryos, with fusion regions indicated with dashed rectangles and magnified below. Ectopic chondrocytes are observed along the mutant ceratohyal cartilage at 60 hpf, which then expand to fuse with Meckel's cartilage by 4 dpf. (B) Confocal imaging of the cartilage marker *sox10*:*dsRed* and perichondrium marker *trps1*:*GFP* in control and three mutants with severe fusion, mild fusion, or ectopic outgrowth of ceratohyal without fusion. Boxed regions are magnified below, and the merged and single *trps1*:*GFP* channels are shown for the highest magnification. The fusion sites are shown by yellow arrows, *trps1*:*GFP*^{high}; *sox10*:*dsRed*$^{+}$ chondrocytes by white arrows, and *trps1*:*GFP*^{low}; *sox10*:*dsRed*$^{+}$ chondrocytes by arrowheads. (C) Model for cartilage fusion in Irx mutants shows ectopic cartilage outgrowths from the perichondrium resulting in aberrant cartilage bridges between neighboring elements. Ch, ceratohyal; Hm, hyomandibula; M, Meckel's; Pq, palatoquadrate. Scale bars: 50 µm.

arch CNCCs in zebrafish *h3f3a* mutants was also found to correlate with loss of the jaw joint in some cases (Cox et al., 2012).

A particular advantage of the zebrafish system is the higher complexity of Irx clusters, thus allowing us to obtain and study genotypic combinations with severe early defects, as well as milder combinations with later skeletal fusions. We find that co-injection of Cas9 and guide RNAs targeting multiple genes can result in independent mutations in up to three linked genes in a single injection, thus demonstrating feasibility of gene editing of complex gene loci in zebrafish. The comprehensive series of Irx cluster mutations we have created should also be a useful resource for disentangling requirements of Irx genes in a diversity of other organ systems.

MATERIALS AND METHODS

Zebrafish lines

All experiments on zebrafish (*Danio rerio*) were approved by the Institutional Animal Care and Use Committee at the University of

Development (2021) 148, dev197244. doi:10.1242/dev.197244

Southern California (Protocol 20771). Previously published lines include *Tg(sox10:dsRed)*^{el10Tg}, *Tg(trps1:GFP)*^{j127aGt} (Talbot et al., 2010), *SAGp11A* (*irx7*:*GFP*), *irx7*^{el540} and *irx5a*^{el576} (Askary et al., 2015), *Tg(~3.4her5:EGFP)*^{ne1911} (Tallafuss and Bally-Cuif, 2003), and *Tg(isl1:EGFPCAAX)*^{fh474} (Barsh et al., 2017). We generated mutant lines using CRISPR/Cas9 editing as previously published (Hwang et al., 2013). We designed sgRNAs within or upstream of the homeobox domain (Fig. 1A, Table S1). The XbaI-digested pT3TS-nCas9n plasmid (Addgene plasmid #46757, deposited by Wenbiao Chen) was used as a template to transcribe Cas9 mRNA with the T3 mMESSAGE kit (Invitrogen). We transcribed sgRNAs from PCR-generated templates using the MEGAscript T7 Kit (Thermo Fisher Scientific). One-cell-stage embryos were injected with a mix of 100 ng/µl Cas9 mRNA and 50 ng/µl of each gene-specific sgRNA. Up to three genes were targeted simultaneously. Injected embryos were raised and founders identified by genotyping progeny for deletions and/or insertions using PCR and restriction digestion (see Table S1 for genotyping assays).

Generation of *IrxAa* alleles

To generate *Irx4a* alleles, 19 injected animals were screened and 18/19 (95%) P0 s carried germline mutations, with an average of 0.95 independent alleles for each P0. Of these, 48% carried single-mutant alleles, 33% carried double-mutant alleles, and 19% carried triple-mutant alleles. Of the triple-mutant alleles, 1/10 (10%) contained out-of-frame alleles for each gene and was used for further phenotypic analysis (*irx4a*^{el832} *irx2a*^{el831} *irx1a*^{el830}). The final founder frequency to create the *IrxAa* allele was 1/19 (5.3%).

Generation of *IrxAb* alleles

To generate *IrxAb* alleles, four injected animals were screened and 4/4 (100%) P0 s carried germline mutations, with an average of 1.625 independent alleles for each P0. Of these, 54% carried single-mutant alleles and 46% carried double-mutant alleles. Of the double-mutant alleles, 3/4 (75%) contained out-of-frame alleles for each gene and one was selected for further phenotypic analysis (*irx4b*^{el834} *irx1b*^{el833}). The final founder frequency to create the *IrxAa* alleles was 3/4 (75%).

Generation of *IrxBa* alleles

To generate *IrxBa* alleles, *irx3a* and *irx6a* guides were injected into zebrafish heterozygous for the *irx5a el576* mutant allele. Twenty-three injected animals were screened and 18/23 (78%) P0s carried germline mutations for *irx3a* and/or *irx6a*, with an average of 0.36 independent alleles for each P0. Of these, 52% carried single-mutant alleles in the absence of *irx5a*, 27% carried single-mutant alleles in the presence of *irx5a*, 9% carried double-mutant alleles in the absence of *irx5a*, and 12% carried triple-mutant alleles. Of the triple-mutant alleles, 1/4 (25%) contained out-of-frame alleles for each gene and was used for further phenotypic analysis (*irx6a*^{el836} *irx5a*^{el576} *irx3a*^{el835}). The final founder frequency to create the *IrxBa* allele was 1/23 (4.3%).

Generation of *IrxBb* alleles

To generate *IrxBb* alleles, five injected animals were screened and 5/5 (100%) P0s carried germline mutations, with an average of one independent allele for each P0. Of these, 100% carried single-mutant alleles and 0% carried double-mutant alleles. To generate double-mutant alleles, progeny from the *irx5b*^{el722} founder carrying an out-of-frame deletion was injected with guides targeting *irx3b*. One P0 was screened to identify a double-mutant allele (100%) containing out-of-frame alleles for each gene (*irx5b*^{el722} *irx3b*^{el837}).

Quintuple heterozygous zebrafish were genotyped every generation for every mutation within each cluster to ensure that recombination had not taken place between loci. Across multiple generations, we did not detect any recombination events.

Skeletal and muscle staining

Alcian Blue and Alizarin Red staining of cartilage and bone was performed as previously described (Walker and Kimmel, 2007). Briefly, larvae were fixed for 1 h in 2% paraformaldehyde (PFA) in PBS at room temperature, washed, and stained overnight in an Alcian Blue solution. Larvae were then rehydrated, bleached with 3% hydrogen peroxide, washed, and stained with an Alizarin Red solution for 30 min. Stained embryos were washed and transferred to a 50% glycerol solution for long-term storage. For muscle staining, larvae were fixed overnight in 4% PFA, washed in PBS, permeabilized overnight in 1% Triton X-100 in PBS, stained with Alexa Fluor 674 phalloidin (Molecular Probes, A22287) at 1:100 overnight, and washed in PBS before imaging.

Imaging

Whole-mount larval skeletons were imaged with a Leica S8APO microscope, and dissected flat-mount skeletons were imaged with a Leica DM2500 microscope. Fluorescent embryos were imaged on a Zeiss LSM800 confocal microscope. All fluorescence images are maximal intensity projections processed with ImageJ. Brightfield images and fluorescence images were further modified for size and level with Adobe Photoshop CS6. To image zebrafish from pharyngula to larval stages, zebrafish carrying transgenic lines were selected between 22 and 24 hpf and individually housed in 24-well plates. Sorted zebrafish were moved to a 22°C incubator at 24 hpf to slow development, and each animal was repeatedly imaged at 36 hpf, 60 hpf, 3 dpf and 4 dpf. To visualize the jaw gape phenotype, 6 dpf zebrafish were embedded in 2% methylcellulose under minimal tricaine dosage to slow zebrafish but enable jaw movement. Movies were taken with a Zeiss Stemi 305 microscope using Zeiss Labscope software. To score dorsal curvature and swimming defects, individually housed animals were imaged at 3 dpf and movies were taken at 4 and 5 dpf using an Apple iPhone 10. Videos were trimmed and annotated using iMovie (Apple).

In situ hybridization and immunofluorescence

Probes for *sox10* (Dutton et al., 2008), *dlx2a* (Akimenko et al., 1994), and *irx1b* and *irx7* (Askary et al, 2015) were previously published. The probe for *irx3a* was amplified from zebrafish cDNA using Phusion High-Fidelity DNA Polymerase (New England BioLabs) with primers GCCATTGTA-CACAGGACATGC (*irx3a*-F) and AGACTACTTGGCCTGACAGC (*irx3a*-R). The PCR product was cloned into pCR Blunt II Topo (Thermo Fisher Scientific), and RNA probe was synthesized from linearized plasmid using Sp6 polymerase and dinitrophenol (DNP)-labeled nucleotides (Roche). Colorimetric and fluorescence *in situ* hybridizations were performed as previously described (Zuniga et al., 2010). Whole-mount immunofluorescence was performed with a mouse anti-phospho-Histone H3 (Ser10) antibody (Millipore Sigma, 05-1336) and a rabbit anti-Active Caspase-3 antibody (BD Pharmingen, 559565). Briefly, dechorionated *sox10*:*dsRed*$^{+}$ embryos were sorted, fixed overnight in 2% PFA in PBS, and washed in PBS. Embryos were permeabilized with ice-cold acetone for 7 min, blocked in 2% goat serum in PBDTx (PBS with 1% bovine serum albumin, 1% DMSO, 0.1% Triton X-100) for 4 h, and incubated overnight in primary antibody at 4°C. Embryos were washed several times with PBDTx and stained with secondary antibodies Alexa Fluor 488 goat anti-rabbit IgG (Thermo Fisher, A-11008) and Alexa Fluor 674 goat anti-mouse IgG1 (Thermo Fisher, A-21240) at 1:300 overnight and washed in PBS. Colorimetric *in situ* hybridizations were imaged on a Leica S8APO microscope, and fluorescence-stained embryos were imaged on a Zeiss LSM800 confocal microscope.

Phenotyping and statistics

Except where indicated, all phenotypes were scored blindly from quintuple heterozygous in-crosses, followed by genotypic analysis. To analyze the distribution of genotypes within a given phenotype, Chi-squared analysis was performed using Excel. After Bonferroni correction, significance was defined as $P<0.01$ based on $P<0.05$ for each of the five genotype categories. Using GraphPad's Prism, an unpaired *t*-test was performed to determine whether there is a genetic interaction between *IrxBa* and *IrxBb* for ceratobranchial cartilage loss, and $P<0.05$ was assigned as significant. In all figures, exact *P*-values are listed given the arbitrary nature of the 0.05 cut-off value. The number of *sox10*:*dsRed*$^{+}$, pHH3^{+} and Caspase-3^{+} cells within the first, second and posterior pharyngeal arches were manually counted using ImageJ. Control and mutant cell counts were compared using a two-tailed non-parametric Student's *t*-test.

Acknowledgements
We thank Megan Matsutani and Jennifer DeKoeyer Crump for fish care, and Cecilia Moens for sharing the *Tg(isl1:eGFPCAAX)*^{fh474} zebrafish line.

Competing interests
The authors declare no competing or financial interests.

Author contributions
Conceptualization: J.G.C.; Methodology: D.T.F., P.P.; Investigation: D.T.F., P.P., R.C., C.-Y.L., J.G.C.; Resources: P.P., J.G.C.; Writing - original draft: D.T.F., J.G.C.; Writing - review & editing: D.T.F., J.G.C.; Visualization: D.T.F., J.G.C.; Supervision: J.G.C.; Project administration: J.G.C.; Funding acquisition: D.T.F., J.G.C.

Funding
Funding was provided by the National Institute of Dental and Craniofacial Research (R35 DE027550 to J.G.C.), a Helen Hay Whitney Foundation fellowship (D.T.F.), and the Howard Hughes Medical Institute Hanna H. Gray Program (D.T.F.). Deposited in PMC for release after 12 months.

Peer review history
The peer review history is available online at https://journals.biologists.com/dev/article-lookup/doi/10.1242/dev.197244

References

Akimenko, M. A., Ekker, M., Wegner, J., Lin, W. and Westerfield, M. (1994). Combinatorial expression of three zebrafish genes related to distal- less: part of a homeobox gene code for the head. *J. Neurosci.* **14**, 3475-3486. doi:10.1523/JNEUROSCI.14-06-03475.1994

Anselme, I., Laclef, C., Lanaud, M., Rüther, U. and Schneider-Maunoury, S. (2007). Defects in brain patterning and head morphogenesis in the mouse mutant Fused toes. *Dev. Biol.* **304**, 208-220. doi:10.1016/j.ydbio.2006.12.025

Askary, A., Mork, L., Paul, S., He, X., Izuhara, A. K., Gopalakrishnan, S., Ichida, J. K., McMahon, A. P., Dabizljevic, S., Dale, R. et al. (2015). Iroquois proteins promote skeletal joint formation by maintaining chondrocytes in an immature state. *Dev. Cell* **35**, 358-365. doi:10.1016/j.devcel.2015.10.004

Barsh, G. R., Isabella, A. J. and Moens, C. B. (2017). Vagus motor neuron topographic map determined by parallel mechanisms of *hox5* expression and time of axon initiation. *Curr. Biol.* **27**, 3812-3825. doi:10.1016/j.cub.2017.11.022

Bonnard, C., Strobl, A. C., Shboul, M., Lee, H., Merriman, B., Nelson, S. F., Ababneh, O. H., Uz, E., Güran, T., Kayserili, H. et al. (2012). Mutations in IRX5 impair craniofacial development and germ cell migration via SDF1. *Nat. Genet.* **44**, 709-713. doi:10.1038/ng.2259

Cain, C. J., Gaborit, N., Lwin, W., Barruet, E., Ho, S., Bonnard, C., Hamamy, H., Shboul, M., Reversade, B., Kayserili, H. et al. (2016). Loss of Iroquois homeobox transcription factors 3 and 5 in osteoblasts disrupts cranial mineralization. *Bone Rep.* **5**, 86-95. doi:10.1016/j.bonr.2016.02.005

Cavodeassi, F., Modolell, J. and Gómez-Skarmeta, J. L. (2001). The Iroquois family of genes: from body building to neural patterning. *Development* **128**, 2847-2855. doi:10.1242/dev.128.15.2847

Cox, S. G., Kim, H., Garnett, A. T., Medeiros, D. M., An, W. and Crump, J. G. (2012). An essential role of variant histone H3.3 for ectomesenchyme potential of the cranial neural crest. *PLoS Genet.* **8**, e1002938. doi:10.1371/journal.pgen.1002938

David, N. B., Saint-Etienne, L., Tsang, M., Schilling, T. F. and Rosa, F. M. (2002). Requirement for endoderm and FGF3 in ventral head skeleton formation. *Development* **129**, 4457-4468. doi:10.1242/dev.129.19.4457

Dutton, J. R., Antonellis, A., Carney, T. J., Rodrigues, F. S., Pavan, W. J., Ward, A. and Kelsh, R. N. (2008). An evolutionarily conserved intronic region controls the spatiotemporal expression of the transcription factor Sox10. *BMC Dev. Biol.* **8**, 105. doi:10.1186/1471-213X-8-105

Gehrke, A. R., Schneider, I., de la Calle-Mustienes, E., Tena, J. J., Gomez-Marin, C., Chandran, M., Nakamura, T., Braasch, I., Postlethwait, J. H., Gómez-Skarmeta, J. L. et al. (2015). Deep conservation of wrist and digit enhancers in fish. *Proc. Natl. Acad. Sci. USA* **112**, 803-808. doi:10.1073/pnas.1420208112

Gomez-Skarmeta, J., de La Calle-Mustienes, E. and Modolell, J. (2001). The Wnt-activated Xiro1 gene encodes a repressor that is essential for neural development and downregulates Bmp4. *Development* **128**, 551-560. doi:10.1242/dev.128.4.551

Grotewold, L. and Rüther, U. (2002). The Fused toes (Ft) mouse mutation causes anteroposterior and dorsoventral polydactyly. *Dev. Biol.* **251**, 129-141. doi:10.1006/dbio.2002.0817

Hwang, W. Y., Fu, Y., Reyon, D., Maeder, M. L., Tsai, S. Q., Sander, J. D., Peterson, R. T., Yeh, J.-R. J. and Joung, J. K. (2013). Efficient genome editing in zebrafish using a CRISPR-Cas system. *Nat. Biotechnol.* **31**, 227-229. doi:10.1038/nbt.2501

Kim, K.-H., Rosen, A., Bruneau, B. G., Hui, C.-C. and Backx, P. H. (2012). Iroquois homeodomain transcription factors in heart development and function. *Circ. Res.* **110**, 1513-1524. doi:10.1161/CIRCRESAHA.112.265041

Li, D., Sakuma, R., Vakili, N. A., Mo, R., Puviindran, V., Deimling, S., Zhang, X., Hopyan, S. and Hui, C.-C. (2014). Formation of proximal and anterior limb skeleton requires early function of Irx3 and Irx5 and is negatively regulated by Shh signaling. *Dev. Cell* **29**, 233-240. doi:10.1016/j.devcel.2014.03.001

McDonald, L. A., Gerrelli, D., Fok, Y., Hurst, L. D. and Tickle, C. (2010). Comparison of Iroquois gene expression in limbs/fins of vertebrate embryos. *J. Anat.* **216**, 683-691. doi:10.1111/j.1469-7580.2010.01233.x

Peters, T., Ausmeier, K., Dildrop, R. and Rüther, U. (2002). The mouse Fused toes (Ft) mutation is the result of a 1.6-Mb deletion including the entire Iroquois B gene cluster. *Mamm. Genome* **13**, 186-188. doi:10.1007/s00335-001-2142-7

Piotrowski, T., Ahn, D.-G., Schilling, T. F., Nair, S., Ruvinsky, I., Geisler, R., Rauch, G.-J., Haffter, P., Zon, L. I., Zhou, Y. et al. (2003). The zebrafish van gogh mutation disrupts tbx1, which is involved in the DiGeorge deletion syndrome in humans. *Development* **130**, 5043-5052. doi:10.1242/dev.00704

Satija, R., Farrell, J. A., Gennert, D., Schier, A. F. and Regev, A. (2015). Spatial reconstruction of single-cell gene expression data. *Nat. Biotechnol.* **33**, 495-502. doi:10.1038/nbt.3192

Talbot, J. C., Johnson, S. L. and Kimmel, C. B. (2010). hand2 and Dlx genes specify dorsal, intermediate and ventral domains within zebrafish pharyngeal arches. *Development* **137**, 2507-2517. doi:10.1242/dev.049700

Tallafuß, A. and Bally-Cuif, L. (2003). Tracing of her5 progeny in zebrafish transgenics reveals the dynamics of midbrain-hindbrain neurogenesis and maintenance. *Development* **130**, 4307-4323. doi:10.1242/dev.00662

Tan, Z., Kong, M., Wen, S., Tsang, K. Y., Niu, B., Hartmann, C., Chan, D., Hui, C.-C. and Cheah, K. S. E. (2020). IRX3 and IRX5 inhibit adipogenic differentiation of hypertrophic chondrocytes and promote osteogenesis. *J. Bone Miner. Res.* **35**, 2444-2457. doi:10.1002/jbmr.4132

Tao, H., Lambert, J.-P., Yung, T. M., Zhu, M., Hahn, N. A., Li, D., Lau, K., Sturgeon, K., Puviindran, V., Zhang, X. et al. (2020). IRX3/5 regulate mitotic chromatid segregation and limb bud shape. *Development* **147**, dev180042. doi:10.1242/dev.180042

Tena, J. J., Alonso, M. E., de la Calle-Mustienes, E., Splinter, E., de Laat, W., Manzanares, M. and Gómez-Skarmeta, J. L. (2011). An evolutionarily conserved three-dimensional structure in the vertebrate Irx clusters facilitates enhancer sharing and coregulation. *Nat. Commun.* **2**, 310. doi:10.1038/ncomms1301

van der Hoeven, F., Schimmang, T., Volkmann, A., Mattei, M. G., Kyewski, B. and Ruther, U. (1994). Programmed cell death is affected in the novel mouse mutant Fused toes (Ft). *Development* **120**, 2601-2607. doi:10.1242/dev.120.9.2601

Veitch, E., Begbie, J., Schilling, T. F., Smith, M. M. and Graham, A. (1999). Pharyngeal arch patterning in the absence of neural crest. *Curr. Biol.* **9**, 1481-1484. doi:10.1016/S0960-9822(00)80118-9

Walker, M. B. and Kimmel, C. B. (2007). A two-color acid-free cartilage and bone stain for zebrafish larvae. *Biotech. Histochem.* **82**, 23-28. doi:10.1080/10520290701333558

Zuniga, E., Stellabotte, F. and Crump, J. G. (2010). Jagged-Notch signaling ensures dorsal skeletal identity in the vertebrate face. *Development* **137**, 1843-1852. doi:10.1242/dev.049056